A Particle Seeding Apparatus for Cryogenic Flow Visualization

Celik, D., NHMFL
Smith, M.R., NHMFL
Van Sciver, S.W., NHMFL/FAMU-FSU College of Engineering

A particle seeding apparatus to create neutrally buoyant solid particles in liquid helium (He I and He II) by injecting a mixture of liquid hydrogen-deuterium has been developed and successfully tested as part of a flow visualization experiment. The apparatus consists of a liquid cavity to hold the liquid hydrogen-deuterium mixture, a vacuum jacket, a plain orifice atomizer, a needle valve, a solenoid valve, heaters and temperature sensors. The needle valve, which is coated with indium to prevent any leaks, closes the gate between liquid mixture and helium, and operates via a solenoid. Heaters in the can control the temperature of the liquid mixture. Temperature is monitored by silicon diode temperature sensors placed on the can. Tests have been performed inside a glass cryostat for visual inspection, and have been recorded using a black and white video camera and a camera equipped with a macro lens.

Appropriate liquid hydrogen-deuterium mixture density is found by controlling the initial gas pressures in the gas measuring cylinders. By neglecting the contraction of particles during solidification, and by considering the fact that mass is a preserved quantity, initial gas pressures are related to final liquid densities in the following way:

$$P_H = \frac{\rho_H RT(\rho_D - \rho_{mix})}{W_H(\rho_D - \rho_H)}\left(\frac{V_{mix}}{V_c}\right) \text{ and } \quad P_D = \frac{\rho_D RT(\rho_{mix} - \rho_H)}{W_D(\rho_D - \rho_H)}\left(\frac{V_{mix}}{V_c}\right)$$

where, V is volume, ρ is liquid density, P is gas pressure, T is gas temperature, R is the universal gas constant, W is molecular weight, and the term V_C is the volume of the gas measuring cylinder the indices H, D and mix represent hydrogen, deuterium and the mixture, respectively.

For a specific nozzle, velocity of the liquid at the nozzle exit is the only changeable parameter affecting the particle size. Therefore, a relation for the nozzle exit velocity is derived based on the energy equation along a streamline:

$$U_E = \sqrt{2g\left[\frac{P_{mix} - P_E}{\gamma} - (h_f + h_s)\right]}$$

where g is the gravitational acceleration, γ is the specific gravity, P_{mix} is the pressure over the liquid mixture. The exit pressure P_E is assumed to be equal to the saturated vapor pressure of liquid helium. h_f and h_s are, respectively, the total head loss terms due to friction and the cross section changes that the liquid encounters along the atomizer.

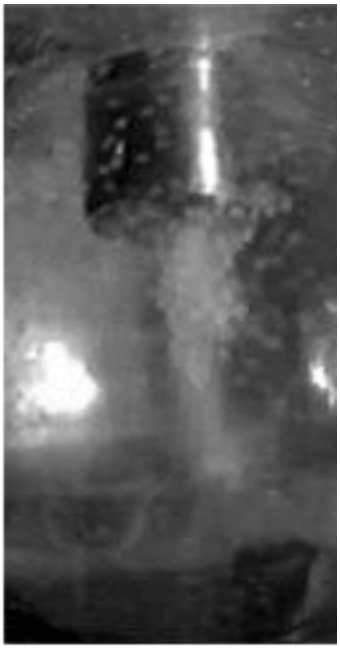

Figure 1. Liquid hydrogen jet issuing into liquid helium.

Depending on the flow velocity inside the nozzle, atomization with different particle sizes has been observed (see Figure 1). Additionally, particle size growth due to the collisions among particles and particles sticking on the glass cryostat have also been noticed. Particle size distribution in terms of nozzle configuration and exit velocity remains to be determined.

Experimental Investigation of the Thermal Conductance in Niobium Samples for Superconducting RF Cavities

Smith, M.R., NHMFL
Zhang, T., NHMFL/FAMU-FSU College of Engineering
Xiang, Y., NHMFL
Van Sciver, S.W., NHMFL/FAMU-FSU College of Engineering

We have measured the overall thermal conductance between typical niobium samples for RF cavity application and He II. The temperature range is 1.7 K to 2.1 K, with heat flux as high as 1000 W/m^2. The test sample is circular plate, 85 mm in diameter and it is mounted to a vacuum can via indium seals. Two 10 mm thick G-10 flanges clamp the sample in place and reduce the heat flux in the radial direction. Another two 5mm thick stainless steel flanges provide mechanical support for the bolts. On the vacuum side, a 60 mm diameter heater is mounted on the sample to supply the heat flux. All the dimensions, including the thickness, are much less than the diameter, allowing us to treat the heat transfer approximately as one-dimensional along the axial direction.

Table 1. Fit parameters for overall thermal conductance.

Exposed Surface	α [kW/m^{2}K$^{1+\beta}$]	β
Niobium	0.955	3.54
Titanium	0.363	2.99
Copper	0.0404	0.447

Three kinds of samples were measured: (1) Niobium with thin layer of titanium; (2) Pure niobium chemically etched from the first sample to remove the titanium layer; (3) Niobium with thick copper layer (~3 mm) by a plasma spraying technique at 200°C, with 3-6% porosity by volume. The results indicate that the temperature difference between the upper surface and the He II bath is proportional to the heat flux up to 500 W/m^2, above that the departure from linear behavior appears. Figure 1 displays the overall thermal conductance of the three samples. Compared to the pure niobium sample, the thin titanium layer decreases the thermal conductance by nearly a factor of three. Most interesting, the sample with copper layer shows very low thermal conductance, which is almost two orders of magnitude lower than that of pure niobium. The mechanism for such a phenomenon is not clear at this time, with possible explanations duo to porosity, oxidation layer on the surface, and the bimetallic interfaces. To anticipate the effect of temperature on the conductance of the three samples, the data shown in Figure 1 are fit to the power law, $k_{eff}=\alpha?T^{\beta}$, with α and β summarized in Table 1.

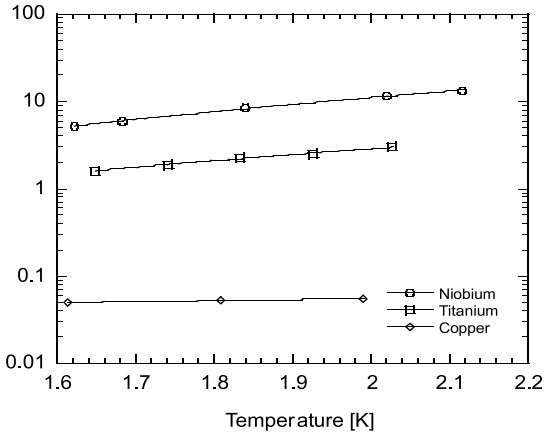

Figure 1. Thermal conductance for niobium samples under three surface conditions.

Flow in Horizontal Two Phase He II/Vapor

Van Sciver, S.W., NHMFL/FAMU-FSU College of Engineering
Panek, J.S., NHMFL/FAMU-FSU College of Engineering
Celik, D., NHMFL

We consider the problem of a stratified two phase He II/vapor flow constrained to a horizontal channel. Heat transport through the channel is by either counterflow in the bulk He II and forced flow in both the vapor and the liquid. Heat exchange between the two phases is by evaporation or condensation.

The solution of this problem can be obtained by use of the differential form for the one-dimensional energy equation for stratified flow,

$$\frac{dy}{dz}+\frac{1}{\rho_l g}\frac{dp_v}{dz}=-\frac{u_l}{g}\frac{du_l}{dz}+\frac{dh_l}{dz} \qquad (1)$$

where the first term on the right hand side is due to fluid acceleration. dh_l/dz is the head loss due to viscous drag along the channel. Equation can be reduced to a differential equation for the liquid slope as it depends on the relative velocities of the two phases,

$$\frac{dy}{dz}=-\frac{2}{\rho_l g D_h}\left(C_{fl}\rho_l u_l^2 \pm C_{fv}\rho_v u_v^2\right) \qquad (2)$$

where C_{fl} and C_{fv} are the liquid and vapor friction factors, respectively and D_h is the hydraulic diameter. Note that Eq. (2) predicts either positive or negative sloping interface dependent on the relative values of the kinetic energy density of the liquid and vapor. If heat and mass flow are parallel, $u_l > 0$, $u_v > 0$, the slope will become more positive relative to the isothermal case. On the other hand, if heat and mass flow are anti-parallel, the slope will become more negative.

For the special case where $u_v = 0$, then a measurement of the slope will yield C_{fl}. Figure 1 displays the experimental measurement of the liquid level differences, under isothermal conditions for mass flow rates up to +/- 2 g/s. During forced flow condition, the level on the upstream side increases and on the downstream side decreases; however, the average level remains approximately unchanged. The results displayed in Figure 1 are fit to Eq. (2) with the corresponding value to a friction factor of $C_{fl} = 0.0057$+/- 0.0006. This value is consistent with the friction factor calculated for the Blausius correlation, $C_f = 0.079/\mathrm{Re}^{1/4}$, for the range of Reynolds number accessed by the experiment ($10^4 < \mathrm{Re} < 10^5$).

Figure 2 displays the magnitude of the level change versus liquid mass flow rate for different conditions with finite T across the channel. In this case, the vapor flow rate is non-zero. These experiments are performed by first establishing the temperature difference for static liquid followed by forced circulation. For the initial condition with static fluid, the liquid interface is sloped upward from warm to cold due to the vapor pressure gradient. In order to attempt to separate the effect of the vapor flow, for the data displayed in Figure 2, this initial slope is subtracted from the measured level change for flowing He II. Thus, in principle, the result should be due only to the hydraulic resistance of the channel and be proportional to m^2. Also plotted in Figure 2 is the predicted level increase based on the isothermal flow measurements, Figure 1. Clearly, the level increase for the non-isothermal flow is significantly larger than expected. Such an increase in level difference could result from a small increase in the T across the channel, however, no measurable shift was observed in the data. Alternatively, the shift could be caused by an increase in the friction factor, but there is no mechanism to justify such a shift. We currently have no explanation for this observation.

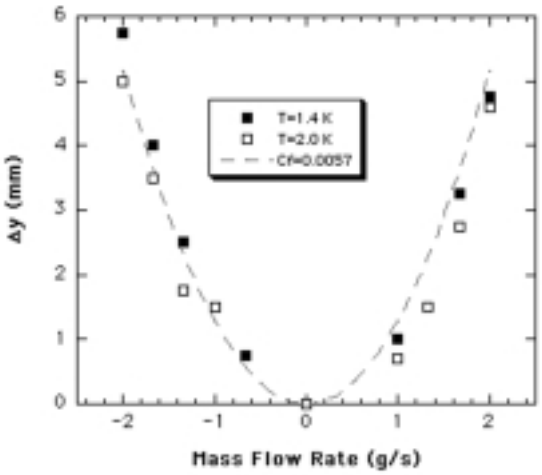

Figure 1. Level change for isothermal flow.

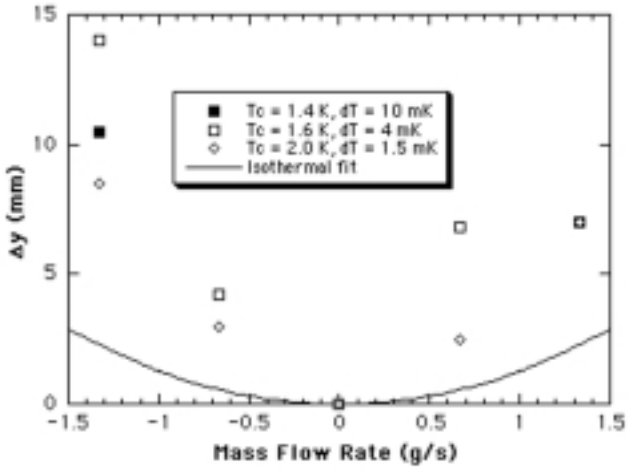

Figure 2. Level change for non-isothermal flow.

In the complete solution to the combined heat and mass transfer one needs to integrate Eq. (5). This requires knowledge of the relationship between *dy/dx* and *dT/dx*, which can be obtained by simultaneous solution of the mass, momentum and energy equations.